Published in final edited form as:
Nat Methods. 2020 February ; 17(2): 163–166. doi:10.1038/s41592-019-0663-9.

An adaptive excitation source for high speed multiphoton microscopy

Bo Li*, **Chunyan Wu**, **Mengran Wang**, **Kriti Charan**, **Chris Xu***
School of Applied and Engineering Physics, Cornell University

Abstract

Optical imaging at high spatial and temporal resolution is important to understand brain function. We demonstrate an adaptive femtosecond excitation source that only illuminates the region of interest. We show that the source reduces the power requirement for two- or three-photon imaging of brain activity in awake mice by more than 30 times. The adaptive excitation source represents a new direction in the development of high speed imaging systems.

High imaging speed is necessary for recording the activity of a large number of neurons[1–7]. Because typical multiphoton microscopes (MPMs) operate at the photon shot-noise limited regime, the maximum number of neurons that can be imaged at high spatial and temporal resolution is fundamentally limited by the maximum permissible average and peak power in biological specimens. Increasing the scanning speed cannot overcome the limit imposed by the "photon budget", i.e., a certain number of signal photons per second per neuron is needed in order to quantify the neuronal activity with a high confidence level. An effective approach to improve the imaging speed is to only image the region of interest (ROI)[8–10]. Since the ROI (e.g., the neurons) may occupy a small fraction of the volume of the mouse brain, a large improvement in imaging speed can be achieved by only illuminating the ROI when compared to conventional raster scanning.

We developed a new laser source that will adapt to the sample under study (i.e., an adaptive excitation source, AES) for high speed imaging of a large number of neurons at low light exposure level. Figs. 1a and 1b show, respectively, the principle and the detailed experimental setup of a MPM with the AES for recording neuronal activity. A high-resolution structural image is obtained by raster scanning of the sample, and the image is processed to find the ROIs. For recording the activity of the neurons, for example, the bright regions of the somas define the ROIs. The ROI information is first converted to a digital

---

***Corresponding author statement:** Bo Li and Chris Xu are both corresponding authors. bl627@cornell.edu; chris.xu@cornell.edu.
Present address:
School of Applied and Engineering Physics, Cornell University, Ithaca, New York, USA.

Author Contributions

C. X. initiated and supervised the study. B. L. designed and performed the experiments and analyzed the data. K. C. contributed to the construction of the fiber amplifiers. C. W. set up the awake imaging system and performed immunohistology and most of the animal surgery. M. W. performed some of the animal surgery. B. L. and C. X. wrote the manuscript.

Competing Financial Interests

The authors declare no competing financial interests.

binary sequence in the time domain and then fed to an arbitrary waveform generator (AWG), which drives a fiber-integrated electro-optic modulator (EOM) and encodes the ROI information onto the pulse pattern. The pulse train (now matched to the sample under study) is amplified to high pulse energy and launched into the laser scanning MPM. The synchronization of scanning and the pulse sequence ensures that the excitation beam will only illuminate the ROIs. By allocating all the permissible laser power on the ROIs (i.e., the laser is completely “turned off” outside the ROIs), the signal generation, and therefore, the imaging speed is improved by the inverse of the volume fraction of the ROIs, without increasing the average or peak power on the sample. A salient feature of our design is that the “unwanted” pulses are removed before the final power amplifier (i.e., the erbium-doped fiber amplifier, EDFA) stage. While modulation of laser power has been done routinely in the past, e.g., blanking the beam or enhancing the dynamic range, the modulation was always performed after the laser or amplifier output (i.e., outside the excitation source)[2,11]. Even though the same adaptive pulse pattern could be obtained by modulation after the laser output, more than 30 times higher output power would be required from the laser (see our experimental results), making the system impractical and expensive. In addition, by placing the modulator inside the excitation source, our design allows a high-speed, low-power (only need to handle < 100 mW), and low-cost fiber-optic modulator to perform the intensity modulation.

Because it is tailored to match the ROIs of the sample under study, the pulse pattern is no longer periodic in time. The main challenge for the AES is to overcome the gain transient in the EDFA, similar to what occurs for burst-mode amplification in telecom and fiber optic systems[12], as illustrated in Supplementary Fig. 1a, before compensation. To equalize the intensity of the output pulses, we setup an automatic feedback loop to pre-compensate the gain transient (Fig. 1b, Supplementary Figs. 1 and 2 and Supplementary Video 1). The intensity of the output pulses is measured by a photo-diode (PD). Based on the measured optical waveform, the AWG output (i.e., the modulation pattern) is adjusted to pre-shape the input pulse train to the EDFA. This process is repeated until the pulse-to-pulse intensity fluctuation is sufficiently reduced. The input and output of the EDFA after different number of iterations are shown in Supplementary Fig. 1b. As shown in Supplementary Fig. 1c, the root-mean-squared (RMS) fluctuation of the pulse intensity at the output of the EDFA decreases with the number of iterations. After 30 iterations, which took a total of approximately 15 seconds to complete, the RMS fluctuation decreased from ~ 17% to ~ 0.005%. The intensity-equalized pulse train is then launched into a photonic crystal rod and undergoes soliton self-frequency shift. The output at 1700 nm are used for three-photon microscopy (3PM), and the solitons at 1840 nm are frequency-doubled to 920 nm for two-photon microscopy (2PM).

3PM requires high pulse energy (e.g., ~ 1 nJ at the focus). Because the maximum average power in biological specimens is limited by sample heating, the repetition rate of the laser for 3PM is typically low (e.g., at 1 to 2 MHz), making 3PM incompatible with high-speed imaging. To demonstrate the improved imaging speed enabled by the AES, we performed *in vivo* 3PM in a densely labeled transgenic mouse. jRGECO1a-labeled neurons in an awake mouse (7 months old, similar data n=9) were imaged at 750 μm beneath the dura with a FOV of 620 μm x 620 μm and a frame rate of 30 Hz (512×512 pixels/frame) (Fig. 2, Supplementary Figs. 3–8 and Supplementary Videos 2 and 3). A comparison of 3PM of neuronal activity with and without AES at the same location is shown in Fig. 2. The photon number per neuron per frame with the AES is more than 30 times higher than that without the adaptive excitation scheme although the same average power of 35 mW is used. More fluorescence time traces are shown in Supplementary Fig. 4. The total recording time was 60 minutes (Supplementary Fig. 5 and Supplementary Video 4). Since the ROIs occupy ~ 4.2 % of the FOV and the fill fraction of the resonant scan is 71.3% in the temporal domain (see Methods), more than 30 times reduction in the average excitation power is achieved, i.e., approximately 1.2 W average power would be required to obtain the same traces if we had used a conventional laser at 32 MHz repetition rate. We performed a longitudinal study and recorded from the same neurons on 6 different days over a period of 4 weeks (Supplementary Figs. 6 and 7). We carried out immunostaining of the brains after imaging and confirmed that there was no measurable tissue damage (Supplementary Fig. 8). The performance demonstrated that the AES enables fast 3-photon activity imaging, and overcomes a significant weakness in 3PM.

We also performed *in vivo* 2PM of the activity of GCaMP6s-labeled neurons[13] in an awake mouse (7 months old, similar data n=2) at 680 μm beneath the dura with a FOV of 700 μm x 700 μm and a frame rate of 30 Hz (512×512 pixels/frame). A comparison of 2PM of neuronal activity with and without AES at the same location is shown in Fig. 3. More fluorescence time traces are shown in Supplementary Fig. 9 and Supplementary Video 5. For ROI imaging, the average power at the surface of the brain was 18 mW. Since the ROIs occupy ~ 3 % of the FOV and the fill fraction of the resonant scan is 71.3% in the temporal domain, approximately 800 mW average power would be required to obtain the same traces if we had used a conventional laser at 32 MHz repetition rate. Such a high average power is beyond the thermal damage threshold (typically ~ 200 mW at 920 nm) of the mouse brain[14]. The demonstrated imaging performance cannot be obtained by external modulation of a conventional femtosecond laser (e.g., the Ti:Sapphire laser) since an average power of ~ 3W would be required at 920 nm. Such a power level is beyond the reach of existing 2-photon excitation sources (see Supplementary Note 1).

While imaging neural activity is the focus of this paper, the ROI can be other structures such as the blood vessels (Supplementary Fig. 10 and and Supplementary Videos 6–7).

Three-dimensional random-access MPM (RAMP) using acousto-optic deflectors (AOD)[15–18] is capable of performing random-access ROI imaging of population of neurons within scattering tissues. To achieve the performance where only the ROIs are illuminated, however, gating of the laser output is still necessary, particularly when the pixel dwell time is comparable to the pixel transit time of the AOD scanner[17]. Therefore, the AES can be combined with RAMP to further improve the excitation efficiency of the system. On the other hand, RAMP suffers several shortcomings, such as complicated dispersion compensation scheme and low deflection efficiency of the AOD (e.g., about 75% for each AOD at ~ 800 nm, even lower for longer wavelengths due to material limitations[17]). A comparison between AES and AOD microscopy is presented in Supplementary Note 2, and shows that imaging with the AES can significantly outperform the best random-access, point-scanning, AOD system when the number of ROIs is large. Another major advantage of the AES is that it can be integrated with any existing laser scanning MPM as long as the pixel clock of the microscope is accessible. For example, we show in Supplementary Fig. 11 structural and ROI imaging of neurons and dendrites using the AES and a commercially available MPM (FV1000MPE, Olympus). No modification of the microscope hardware or software was necessary for performing the experiments.

The low average power used in achieving the imaging results (e.g., 18 mW for 2PM and 35 mW for 3PM) indicates that there is plenty of power budget to further increase the imaging speed using the AES, for example, by using higher speed resonant scanners or polygon scanners. While we have demonstrated imaging of a single plane using the AES, it can be straightforwardly applied to 3-dimensional volumetric imaging by combining with high-speed axial scanning devices such as remote focusing[19,20], opening up exciting new opportunities for high-speed, large scale, volumetric imaging of neuronal activity with cellular resolution.

We demonstrated an AES for imaging neuronal activity with a large FOV, a large penetration depth and a high frame rate while using low average power. Although our main motivation is to improve the speed of activity recording, the concept of the AES represents a new direction in designing an imaging system where the excitation source itself is optimized according to the sample under study. The adaptive excitation technique requires no modification of the microscope hardware, has the same large FOV of a conventional MPM, and works at the excitation wavelengths for both 2PM and 3PM. In fact, the AES can be integrated with any existing MPMs, which will enable easy translation of the technique to the wider imaging community.

Online Methods

Fiber-based AES for 3PM

The source consists of a fiber chirped pulse amplification system at 1,550 nm, and a photonic crystal rod for soliton self-frequency shift (SSFS). A compact, turnkey, fiber-based seed laser (FPL-02CFFT, Calmar) delivered linearly polarized pulses with an average power of 100 mW, a repetition rate of 32 MHz, and a bandwidth [full width at half maximum (FWHM)] of 13.7 nm at 1,550 nm. The pulses were then chirped to 642 ps, with second-order dispersion of –51 ps/nm and third-order dispersion of –2.6 ps/nm^2. A fiber-integrated electro-optic modulator (IOAP-MOD9170-F-F-0, SDL) was used to modulate the chirped pulses according to the ROIs of the sample under study. The adaptive pulses were amplified by a two-stage home-built EDFA and compressed by a grating pair (PC 1200 30×110×16 NIR, Spectrogon). The compressed output has a pulse width of 470 fs (Fig. 1) and an average power of more than 6 W. SSFS was performed in a 44-cm-long, polarization-maintained photonic crystal rod (SC-1500/100-Si-ROD, NKT Photonics) with an effective mode area of 4,400 μm^2 at 1,550 nm. After collimation, a 1,620 nm long-pass filter (BLP01–1648R-25, Semrock) was used to filter out the residual pump. The soliton was shifted to 1,680 nm at an input pulse energy of 1,300 nJ[21]. The pulse width of the soliton was measured to be 64 fs by performing second-order autocorrelation, assuming a sech^2 intensity profile (Fig. 1). The pulse energy of the soliton was 140 nJ. A silicon wafer (uncoated, 2 mm thickness, Edmund Optics) is positioned at the Brewster's angle to pre-compensate the dispersion of the microscope optics. The intensity stability of the soliton pulses was measured using two-photon excited photocurrent in a Si PD. The RMS fluctuation of the soliton pulses was less than 1% when measured for 10 minutes at a sampling rate of 100 kHz. The wavelength stability is measured using a spectrometer. The RMS fluctuation of the center wavelength of the soliton is less than 1 nm when measured for 20 minutes at 2 wavelength scans/s.

Fiber-based AES for 2PM

The same fiber chirped pulse amplification system at 1,550 nm was used as the pump for SSFS. SSFS was performed in a 36-cm-long, polarization-maintained photonic crystal rod (DC-200–70-PM-Yb-ROD, NKT Photonics) with an effective mode area of 2,300 μm^2 at 1,550 nm. After collimation, a 1,720 nm long-pass filter (1720LP/50.8, Omega optical) was used to filter out the residual pump. The soliton was shifted to 1,840 nm, at an input pulse energy of 1,260 nJ. The pulse width of the soliton was measured to be 70 fs by performing second-order autocorrelation, assuming a sech^2 intensity profile (Fig. 1). The pulse energy of the soliton was 110 nJ. Pulses at the wavelength of 920 nm were then obtained by second harmonic generation (SHG) of the soliton source, using a frequency-doubling crystal BiBO ($\theta = 9.8^0$, $\varphi = 0^0$, L= 1 mm, Castech). The pulse energy and pulse duration of the pulses at 920 nm was 60 nJ and 60 fs, respectively. A prism pair (80 cm separation, 10SF10, Newport) was used to pre-compensate the dispersion of the microscope optics. The intensity stability of the SHG pulses was measured using two-photon excited photocurrent in a GaAsP PD. The RMS fluctuation of the SHG pulses was less than 1% when measured for 10 minutes at a sampling rate of 100 kHz.

Feedback loop for compensating the gain transient of the EDFA

A small portion (< 1%) of the light at 1,550 nm after the grating pair was detected by a PD (ET08CFC, Thorlabs). The PD output was low-pass filtered (BBLP-39+, Mini-Circuits) and recorded by a data acquisition card (ATS9371, Alazar technologies). Based on the measured output optical waveform, the AWG (NI PXI-5412, National instrument) output was adjusted to pre-shape the input pulse train to the EDFA. This process was repeated until the pulse-to-pulse intensity fluctuation was sufficiently reduced. The algorithm for adjusting the modulation pattern of the AWG is: $A_{n+1}=A_n * [1 - C * (P_n - <P>) / <P>]$, where P_n is the measured peak power of an output pulse of the nth iteration, <P> is the averaged peak power of all output pulses of the nth iteration, A_n is the AWG modulation amplitude of the nth iteration, A_{n+1} is the AWG modulation amplitude of the (n+1)th iteration, and $C \in (0,1)$ is a constant. 20 to 30 iterations were typically used to equalize the pulse intensity.

Imaging setup

The images were taken with a custom-built multiphoton microscope with a high-numerical aperture objective (Olympus XLPLN25XWMP2, 25X, NA1.05). The signal was epi-collected through the objective and then reflected by a dichroic beam splitter (FF705-Di01, Semrock) to the detectors. We used two PMTs with GaAsP photocathodes (H7422P-40, Hamamatsu) for the fluorescence and third-harmonic generation (THG) signals. For 2PM, the optical filter for the fluorescence signal was centered at 520 nm (FF01–520/60–25, Semrock). For 3PM, a 568-nm dichroic beam splitter (MD568, Thorlabs) was inserted at 45°

to the signal beam path to separate the fluorescence and the THG signal to their respective PMTs. The filters for the fluorescence and THG signal were centered at 630 nm (MF630–69, Thorlabs) and 550 nm (FF01–550/49–25, Semrock), respectively. The mouse was placed on a motorized stage (MP-28, Sutter Instrument). A computer running the ScanImage 5.3 module (Vidrio Technologies) with MATLAB (MathWorks) software was used to control the stage translation and image acquisition. The PMT current was converted to voltage by transimpedance amplifiers (DHPCA-100, Femto, and TIA60, Thorlabs). Analog-to-digital conversion was performed by a data acquisition card (NI5734, National instrument). For depth measurement, the slightly larger index of refraction in brain tissue (1.35 to 1.43 for the cortex), relative to water (~ 1.33), results in an underestimate (5–10%) of the actual imaging depth within the tissue because the imaging depths reported here are the raw axial movement of the objective. A galvo-resonant scanner (RESSCAN-GEN, Sutter Instrument) was used to achieve the frame rate of 30 Hz at 512×512 pixels/frame.

Fill fraction of the resonant scanner

For a resonant scanner, the angular velocity at the edge of the scan field is low and highly nonlinear, and thus, the acquisition is inactive and no pixel is recorded in this region. The ratio between the active acquisition time and the total time of a line is defined as the fill fraction in ScanImage 5.3. In the experiment, the fill fraction was 71.3% in the temporal domain and 90% in the spatial domain. The AES was turned off (i.e., no output pulses) in the inactive regions for data acquisition.

Synchronization of the laser, electro-optical modulation, and microscope

For synchronization, there are two clocks, one from the seed laser source and the other from the resonant scanner of the microscope. The synchronization output of the pulsed seed laser (32 MHz) was used as the sampling clock of the AWG, ensuring synchronization of the laser pulses and the electro-optical modulation. The third harmonic of the synchronization output of the seed laser (i.e., 96 MHz) was used as the sampling clock of the microscope data acquisition. According to the ROI information obtained from the structural image (512 × 512 pixels), 512 binary digital sequences (each sequence corresponds to one line of a frame) were generated by MATLAB and stored in the on-board memory of the AWG. The line clock from the microscope was used as the start trigger of the AWG so that the laser scanning and the electro-optical modulation were synchronized. For activity recording, the repetition rate of the excitation source within the ROI was 32 MHz. For structural imaging, a uniform periodic pulse train with repetition rate of 4 MHz and 2 MHz was used for 2PM and 3PM, respectively. A large number of frames (~ 3000) were averaged to achieve the high signal-to-noise ratio of the structural images.

Image processing for structural imaging and activity recording

Structural images were processed with a median filter of 1–2 pixel radius and then normalized by linear transform of pixel intensities to saturate the brightest 0.2–3% of pixels in each frame. Fluorescence intensity traces were low-pass filtered with a hamming window of a time constant of 0.23 s. All traces with absolute photon counts were raw data without filtering. We determined the baselines of the traces (F_0) by excluding the transients. $\Delta F/F$ traces were then obtained according to the formula $(F - F_0)/F_0$.

Photon counting

To show the absolute signal strength in the unit of photon count rate, pixel values are multiplied by a calibration factor. The calibration factor is obtained by observing the modes in the histogram of images of a uniform fluorescein sample, recorded with a short pixel dwell time such that each pixel typically has one or zero photon.

Animal procedures

All animal experiments and housing procedures were conducted in accordance with Cornell University Institutional Animal Care and Use Committee guidance. We used transgenic mice CamKII-tTA/tetO-GCaMP6s (7 months old, male) for 2PM, transgenic mice C57BL/6J-Tg(Thy1-jRGECO1a)GP8.58Dkim/J (3–7 months old, male) for 3PM of neurons and C57BL/6J (3 months old, male) for 3PM of blood vessels.

Chronic craniotomy

The diameter of the cranial window is 5 mm. For 2PM and 3PM of blood vessels, the window was centered at 2.5 mm lateral and 2 mm posterior from the bregma point. For 3PM of neurons, the window is centered at the bregma point. To reduce the tissue growth under the window for chronic imaging, we used a coverslip assembly consisting of a donut-shaped coverslip (inner diameter 4.5 mm, outer diameter 5.5 mm, laser cut by Potomac Photonics) glued concentrically above a 5 mm diameter coverslip (#1 thickness, Electron Microscopy Sciences; optical glue, Norland Optical Adhesive 68). The circular coverslip fit snugly into the open cranial window and was placed directly onto the intact dura. The donut coverslip on the top was glued to the skull (3M Vetbond tissue adhesive) to keep the 5-mm coverslip pressed against the tissue, displacing as much room for potential tissue growth as possible. We applied multiple thin layers of metabond glue on the exposed skull surrounding the coverslip and positioned the head-bar directly onto the glue. The head-bar was further stabilized with Metabond glue and dental cement covering the skull and the circular coverslip. For all mice, chronic imaging was performed at least 5 days after the surgery for tissue inflammation to disappear, with the animal kept alive after each imaging session. For awake imaging, the mouse was standing in a slippery tube when the head was fixed on a custom-made stereotaxic plate using the metal head-bar holder.

Reporting Summary

Further information on research design is available in the Nature Research Reporting Summary linked to this article.

Data availability

The data that support the findings of this study are available from the corresponding author upon request.

Code availability

The Matlab code for driving the AWG (NI PXI-5412, National instrument) and data acquisition card (ATS9371, Alazar technologies) can be found at https://github.com/Bo-Li-

ORCID-0000-0003-1492-0919/Adaptive-excitation-source-for-high-speed-multi-photon-microscopy.

Statistics and reproducibility

For 3PM of brain activity (Fig. 2, Supplementary Figs. 3–5 and Supplementary Videos 2–4), similar results were obtained from 9 mice (3–7 months old). Longitudinal recording of neuronal activity (Supplementary Figs. 6 and 7) was from 1 mouse (12–17 weeks). For immunohistology (Supplementary Fig. 8), similar results were obtained from 6 mice (3–7 months old). For 2PM of brain activity (Fig. 3, Supplementary Fig. 9 and Supplementary Video 5), similar results were obtained from 2 mice (3 and 7 months old). For compensation of the gain transient (Supplementary Figs. 1 and 2 and Supplementary Video 1), similar results were obtained for more than 30 different image patterns. For 3PM of blood flow (Supplementary Fig. 10 and Supplementary Videos 6 and 7), similar results were obtained from 2 mice (both 3 months old). 2PM of neurons with a commercial MPM (Supplementary Fig. 11) was from 1 mouse (2 months old).

Supplementary Material

Refer to Web version on PubMed Central for supplementary material.

Acknowledgements

We thank members of the Xu research groups (T. Wang, D. Ouzounov, D. sinfeld, C. Huang, X. Yang, A. Mok, F. Xia, Y. Hontani, Y. Qin, N. Akibari, K. Choe, T. Ciavatti and C. Zhuang) for their help. We thank M. Buttolph and L. G. Wright for discussions. This work is partially funded by NIH/NINDS (grant no. U01NS090530 to C.X.), and the National Science Foundation NeuroNex (grant no. DBI-1707312 to C.X.).

References

1. Denk W, Strickler JH & Webb WW Two-photon laser scanning fluorescence microscopy. Science 248, 73–76 (1990). [PubMed: 2321027]
2. Zipfel WR, Williams RM & Webb WW Nonlinear magic: multiphoton microscopy in the biosciences. Nat. Biotechnol. 21, 1369–1377 (2003). [PubMed: 14595365]
3. Helmchen F & Denk W Deep tissue two-photon microscopy. Nat. Meth. 2, 932–940 (2005).
4. Dombeck DA, Khabbaz AN, Collman F, Adelman TL & Tank DW Imaging Large-Scale Neural Activity with Cellular Resolution in Awake, Mobile Mice. Neuron 56, 43–57 (2007). [PubMed: 17920014]
5. Horton NG et al. In vivo three-photon microscopy of subcortical structures within an intact mouse brain. Nat. Photon. 7, 205–209 (2013).
6. Sofroniew NJ, Flickinger D, King J & Svoboda K A large field of view two-photon mesoscope with subcellular resolution for in vivo imaging. eLife 5, e14472 (2016). [PubMed: 27300105]
7. Ouzounov DG et al. In vivo three-photon imaging of activity of GCaMP6-labeled neurons deep in intact mouse brain. Nat. Meth. 14, 388–390 (2017).
8. Papagiakoumou E et al. Scanless two-photon excitation of channelrhodopsin-2. Nat. Meth. 7, 848 (2010).
9. Packer AM, Russell LE, Dalgleish HWP & Häusser M Simultaneous all-optical manipulation and recording of neural circuit activity with cellular resolution in vivo. Nat. Meth. 12, 140 (2014).
10. Pnevmatikakis Eftychios A et al. Simultaneous Denoising, Deconvolution, and Demixing of Calcium Imaging Data. Neuron 89, 285–299 (2016). [PubMed: 26774160]

11. Yang R, Weber TD, Witkowski ED, Davison IG & Mertz J Neuronal imaging with ultrahigh dynamic range multiphoton microscopy. Sci. Rep. 7, 5817 (2017). [PubMed: 28725020]
12. Desurvire E, Giles CR & Simpson JR Gain saturation effects in high-speed, multichannel erbium-doped fiber amplifiers at lambda= 1.53 μm. J. Lightwave Tech. 7, 2095–2104 (1989).
13. Chen T-W et al. Ultrasensitive fluorescent proteins for imaging neuronal activity. Nature 499, 295–300 (2013). [PubMed: 23868258]
14. Podgorski K & Ranganathan G Brain heating induced by near-infrared lasers during multiphoton microscopy. J. Neurophysiol. 116, 1012–1023 (2016). [PubMed: 27281749]
15. Reddy GD, Kelleher K, Fink R & Saggau P Three-dimensional random access multiphoton microscopy for functional imaging of neuronal activity. Nat. neurosci. 11, 713–720 (2008). [PubMed: 18432198]
16. Grewe BF, Langer D, Kasper H, Kampa BM & Helmchen F High-speed in vivo calcium imaging reveals neuronal network activity with near-millisecond precision. Nat. Meth. 7, 399–405 (2010).
17. Katona G et al. Fast two-photon in vivo imaging with three-dimensional random-access scanning in large tissue volumes. Nat. Meth. 9, 201–208 (2012).
18. Chavarha M et al. Fast two-photon volumetric imaging of an improved voltage indicator reveals electrical activity in deeply located neurons in the awake brain. bioRxiv, 445064 (2018).
19. Botcherby EJ et al. Aberration-free three-dimensional multiphoton imaging of neuronal activity at kHz rates. PNAS 109, 2919–2924 (2012). [PubMed: 22315405]
20. Weisenburger S et al. Volumetric Ca2+ Imaging in the Mouse Brain Using Hybrid Multiplexed Sculpted Light Microscopy. Cell 177, 1050–1066 (2019). [PubMed: 30982596]

Methods-only References

21. Charan K, Li B, Wang M, Lin CP & Xu C Fiber-based tunable repetition rate source for deep tissue two-photon fluorescence microscopy. Biomedical Opt. Express 9, 2304–2311 (2018).

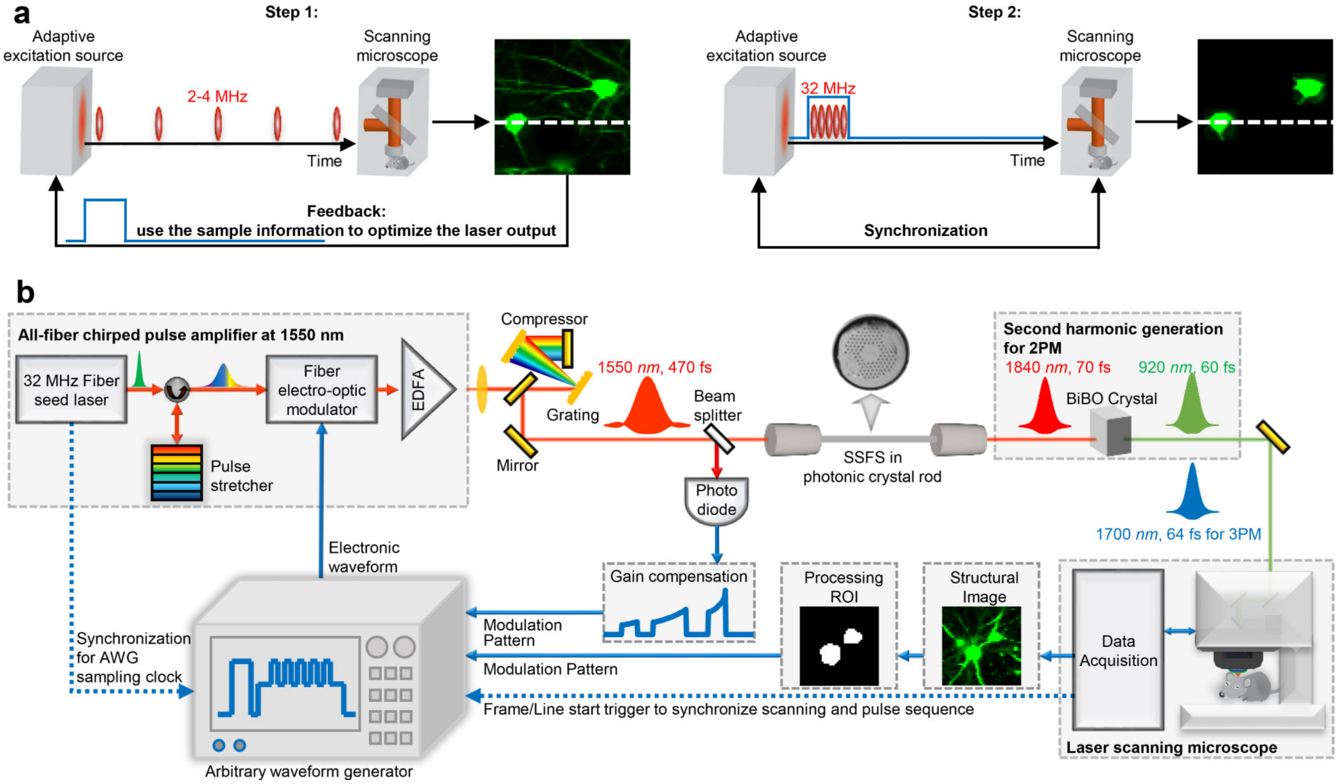

Fig. 1 |. The AES for MPMs.

a, Working principle. The creation of the AES consists of two steps: (1) A high-resolution structural image is obtained by raster scanning of the sample, and the image is processed to find the ROIs, e.g., the neurons, and (2) an adaptive pulse train is generated based on the ROI information. The synchronization of the scanning and the pulse sequence ensures that the excitation beam only illuminates the ROIs. **b**, Experimental setup. The optical path is shown in red and green, and the electrical path is shown in blue. The measured second-order autocorrelation traces are shown at three locations along the optical path. The FWHM of the pulse width (assuming sech^2-intensity profiles) are indicated next to the autocorrelation traces.

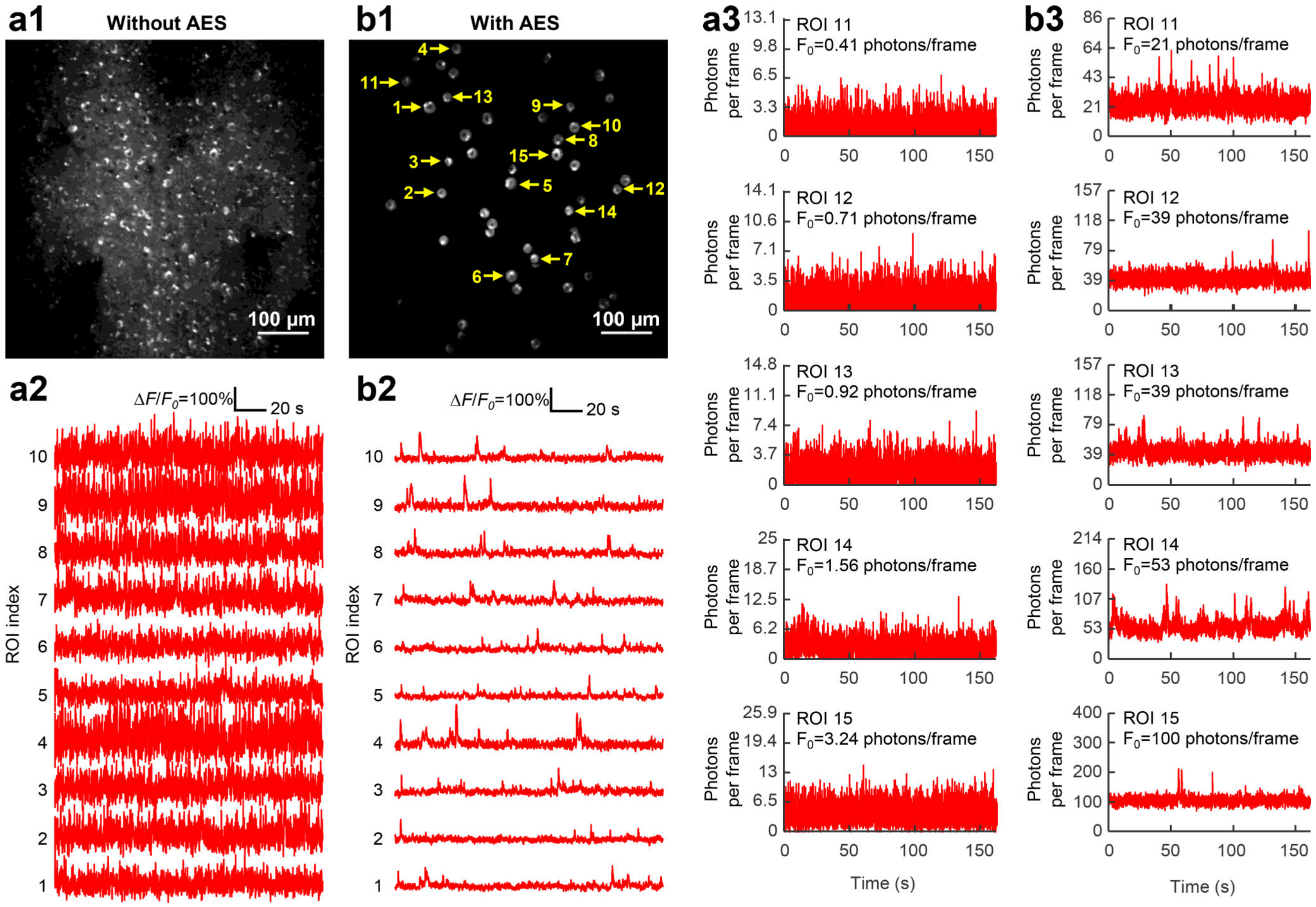

Fig. 2 |. Comparison of 3PM of the spontaneous activity of neurons without (a1, a2, a3) and with (b1, b2, b3) AES at the same location in an awake mouse.

The neurons are located at 750 μm beneath the dura and labeled with jRGECO1a. **a1, b1,** Structural image of neurons. For 3PM without AES, the average power is 35 mW below the objective lens, and the excitation source outputs a uniform, periodic pulse train with a repetition rate of 2 MHz. For 3PM with AES, the average power is also 35 mW. The ROIs were designed to be somewhat larger than the neurons in order to compensate for the motion of the awake mouse (Supplementary Fig. 3 and Supplementary Videos 2 and 3). The repetition rate of the pulses within the ROIs (i.e., when the laser is "on") was 32 MHz, sufficient for high-speed recording of neuronal activity using the resonant scanner. **a2**, **b2**, Spontaneous activity traces recorded from the labeled neurons indicated in **b1**. **a3**, **b3**, Quantitative photon counting of the activity traces of the neurons recorded from the labeled neurons indicated in **b1**. The photon number per neuron per frame with the adaptive excitation (b3) is more than 30 times higher than that without the adaptive excitation (a3). Scale bars, 100 μm. The images have a FOV of 620×620 μm with 512×512 pixels/frame. Scale bars, 100 μm.

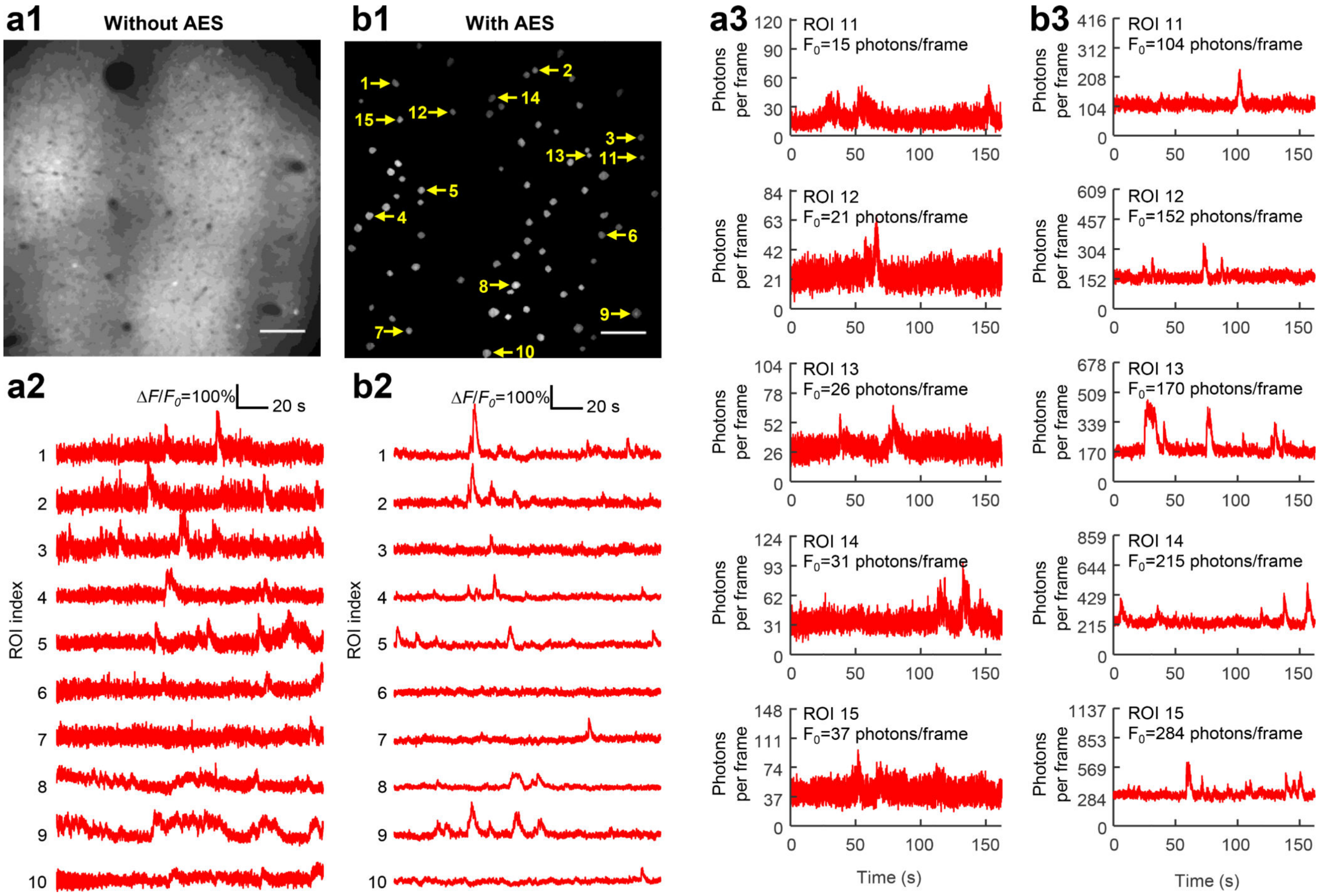

Fig. 3 |. Comparison of 2PM of the spontaneous activity of neurons without (a1, a2, a3) and with (b1, b2, b3) AES at the same location in an awake mouse.

The neurons are located at 680 μm beneath the dura and labeled with GCaMP6s. **a1, b1,** Structural image of neurons. For 2PM without AES, the average power below the objective lens is 80 mW, and the excitation source outputs a uniform, periodic pulse train with a repetition rate of 4 MHz. For 2PM with AES, the average power is 18 mW. The repetition rate of the pulses within the ROIs (i.e., when the laser is “on”) was 32 MHz. **a2**, **b2**, Spontaneous activity traces recorded from the labeled neurons indicated in **b1**. **a3**, **b3**, Quantitative photon counting of the activity traces of the neurons recorded from the labeled neurons indicated in **b1**. The photon number per neuron per frame with the adaptive excitation (b3) is more than 7 times higher than that without the adaptive excitation (a3) even though the average power used for adaptive excitation is ~ 4.5 times lower. Scale bars, 100 μm. The images have a FOV of 700×700 μm with 512×512 pixels/frame. Scale bars, 100 μm.